Available online at www.sciencedirect.com

ScienceDirect

Energy Procedia 94 (2016) 20 – 28

Energy Procedia

13th Deep Sea Offshore Wind R&D Conference, EERA DeepWind'2016, 20-22 January 2016, Trondheim, Norway

Fulfilment of grid code obligations by large offshore wind farms clusters connected via HVDC corridors

A. B. Attya[a,*], O. Anaya-Lara[a], P. Ledesma[b], H. G. Svendsen[c]

[a]*Department of Electronic and Electrical Engineering, University of Strathclyde, Glasgow, UK*

[b]*Department of Electrical Engineering, Charles III University of Madrid, Madrid, Spain*

[c]*Energy Research, SINTEF Energi AS, Trondheim, Norway*

Abstract

The foreseen high penetration levels of wind power will force the systems operators to apply restrictive constraints on wind power plants. The ability of offshore wind clusters, which are connected via HVDC, to fulfill the grid codes, especially those related to voltage stability is investigated. This came in the frame of a project to develop an integrated and practical tool to design offshore wind clusters (EERA-DTOC). The applied case studies examine the system stability during and after severe disturbances, and the compliance with the grid codes. Additionally, this paper explains the applied procedure to utilize the outcomes of Net-OP tool, which proposes an optimized topology to connect the wind power clusters to the interconnected power systems. The integrated simulation environment, namely, PSS/E, is used to implement a highly detailed and dynamic model based on the recommendations of Net-OP tool. The results confirm that wind farm clusters respond to faults and disturbances as desired by the grid codes.

Peer-review under responsibility of SINTEF Energi AS

Keywords: Wind power, Grid integration, Ancillary services, Voltage stability, PSS/E

1. Introduction

Renewable energies continue to make a strong foothold to contribute to the rapidly rising share of energy supply in this decade with wind power accounting for accounting for 39% of the integrated renewable power capacity in 2012 [1]. Future energy plans for several countries count on the massive integration of renewable energies, namely, wind energy. The Danish government has a very ambitious plan to achieve to achieve more than 50% of wind energy penetration, in the installed generation capacity, by the year 2050 [2]. Likewise, there are condensed efforts in the European Union to mitigate carbon emissions, and push nuclear plants to retire. For example, Germany is planning by the end of year 2020 to achieve about 40 GW of wind power installed capacity [3]. However, the

* Corresponding author. Tel.: +44-141-444-7221 ; E-mail address: ayman.attya@strath.ac.uk

Peer-review under responsibility of SINTEF Energi AS

doi:10.1016/j.egypro.2016.09.183

replacement of conventional plants could make the gird highly vulnerable to stability issues, mainly, during frequency drops and voltage dips. This returns to the intermittent nature of wind power, composition of the wind turbine generator (WTG), and its connection methods to the grid. Consequently, grid codes apply strict constraints on the connection of large wind farms to the grid [4]. However, the compliance of future planned offshore wind farm clusters (WFC) with grid codes require further analysis, mainly, when these WFCs are connected via HVDC.

Ancillary services provided by WFCs and grid code requirements are two sides of one coin. In other words, the grid codes specify the role of WFCs during special events (e.g. frequency drop and voltage collapse). In some events, the supportive contribution of WFCs is mandatory, and optional in other cases for the sake of financial incentives. For example, presently, in the French code, the WFCs are not obligated to provide primary reserve [5]. In the United Kingdom code, the WTGs must follow a predefined Low Voltage Ride-through (LVRT) pattern during voltage dips [6]. Generally, this is a dominant trend in the majority of codes; WFCs must provide voltage support while frequency support is optional and financially compensated. The main regimes and services which are defined by grid codes are included in Fig 1-a.

The Designing Tool for Offshore wind farms Clusters (DTOC) aims to provide a user-friendly software which describes the optimum method to connect large capacity offshore wind farms where each group of wind farms forms a cluster [7]. The tool compares between several methods of connection, namely, AC, HVDC or Hybrid, and suggests the best choice based on economic studies. In particular, the energy production and losses are estimated to decide the suitable method of connection to the onshore grids and how the WFCs should be meshed. The accurate execution of this task requires meteorological and technical data, as well as the chronological dominant energy prices in the markets which will be connected to the WFCs. For example, the fixed costs of power electronics converters (PECs) are needed to estimate the costs of HVDC corridors. Likewise, the technical data of the AC and HVDC lines (e.g. impedance parameters and losses factors) are mandatory to estimate the energy losses, and in turn the net energy production. This stage is performed using Net-OP tool [8]. The internal networks of wind farms are designed using a tool called EeFarm II [9]. The inter-array system connecting the WTGs is decided based on a simplified comparison which acknowledges the losses and investment costs of several topologies. The main topologies are Radial (WTGs in strings) and Star (geographically-near a group of WTGs; each WTG is connected independently to the collection platform). The tool also compares the HVDC mutli-terminal groups of WTGs, and WTGs in AC-connected groups, then connected through DC choppers to the collection platform (i.e. hybrid topology). The collection platforms could be connected either through medium voltage AC or DC to central substations to form WFCs [10]. The basic stages of DTOC analysis scheme are briefed in Fig 1-b.

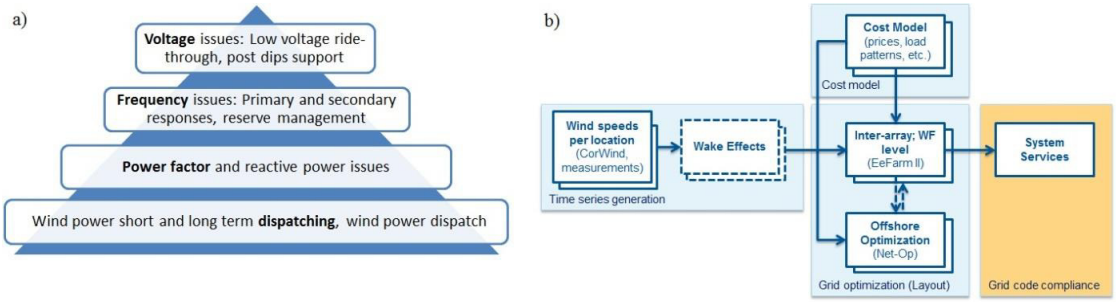

Fig. 1. (a) topics related to grid codes; (b) major packages of the proposed design tool

2. Benchmark system

The examined system represents the major synchronous areas which will be connected directly or indirectly to the three WFCs (overall capacity 3.6 GW equally distributed between WFCs A, B and C). This system is inspired from the outcome of Net-OP tool shown in Fig. 2, which recommended certain topology to connect the three WFCs.

The single line diagram of the test system is shown in Fig. 3. Buses 20, 30, 40 and 50 aggregate the conventional and wind generation (green generators) in Norway, UK, Germany and the Netherlands respectively. The annual average load demand at each bus location is integrated according to real chronological hourly data (i.e. obtained

from Net-Op). Meanwhile, WFCs A, B and C are connected to Buses 101, 102 and 103 respectively. For the sake of simplicity, wind generation is modeled by a single aggregate machine of type 4 (Full rated converter wind turbine generator) at each bus. Likewise, conventional generation is modelled as a single generator with a capacity equal to the generation capacity of the entire region of the bus (the source reactance and resistance, and inertia are assumed to be 0.3 and 0.06 per unit and 6s respectively). Table 1 describes the generation capacities at each bus, and Table 2 includes the aggregate load at each region. A limitation is applied to wind generated power through assuming that the capacity factor of any WFC is not exceeding 55% of its nameplate capacity [2, 3].

The system shown in Fig. 3 contains 12 HVDC corridors which connect the three WFCs to the onshore grids, and connect other commissioned or under construction offshore WFs (e.g. the WFC at Bus 22). In addition, there is a DC link between UK and Norway (future expectation proposed by Net-Op). As an assumption, all the corridors are 1100 kV and have rated capacity of 1500 MVA (values might seem to be high, but this system is dealing with a scenario to be executed after 14 years from now).

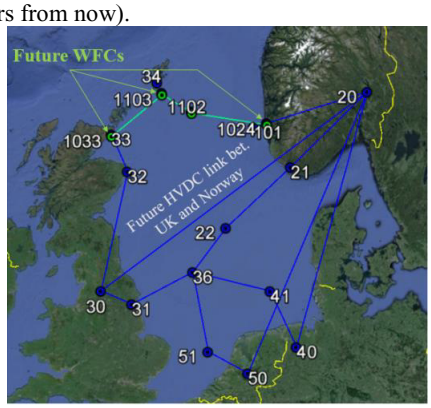

Fig. 2. Geographical layout of the system proposed by Net-OP tool

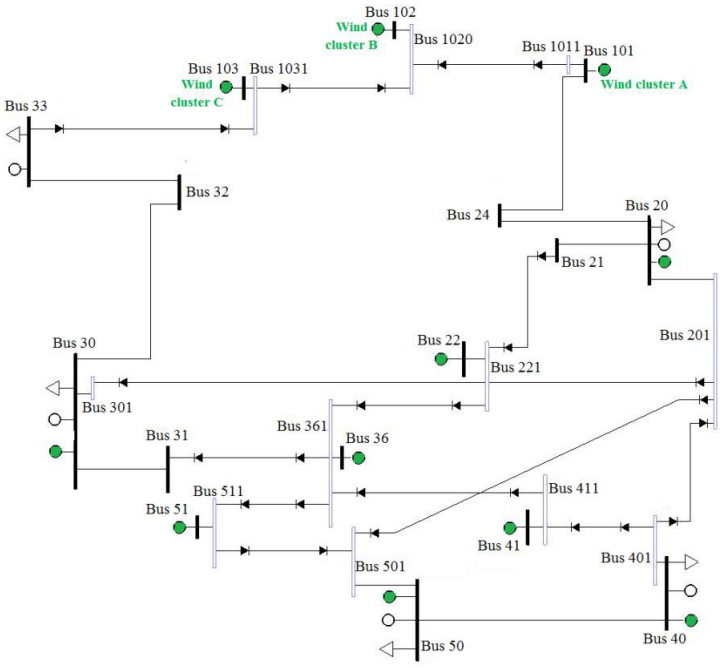

Fig. 3. Benchmark system single line diagram

Table 1. Assumed aggregate conventional and wind generation installed capacities

Aggregate generation (MW)		Onshore wind clusters (MW)	
Bus 20- Norway	31,900	Bus 20-Norway	15,450
Bus 30- UK	82,630	Bus 30-UK	58,320
Bus 33	1000	Bus 40-Germany	73,250
Bus 40- Germany	128,900	Bus 50-Netherlands	18,120
Bus 50- Netherlands	25,460		

Table 2. Assumed aggregate load-demands in the synchronized areas.

Aggregate load (MW)	
Bus 20-Norway	17,352
Bus 30-UK	49,772
Bus 33	49
Bus 40-Germany	72,146
Bus 50-Netherlands	15,868

3. Modelling of the benchmark system and applied faults in PSS/E

This section describes the methodology applied to build the dynamic model of the benchmark system (in PSS/E) based on the *.RAW file from Net-Op tool. Two different approaches are implemented to simulate the fault events. The RAW file of a PSS/E model includes the conventional power flow data of the generators, loads and nodes in the model at the initial steady state.

3.1. Benchmark dynamic model

Comprehensive changes and additions were required to prepare the *.RAW file provided by Net-OP tool to reach an acceptable dynamic model (*.DYR: A file that includes the dynamic models' types and specifications of the integrated generators and converters). One of the problems was the connection of WFCs to HVDC links, as the PSS/E does not accept the connection of a swing bus to an HVDC. To overcome this, a supplementary bus is added at each bus to be connected to HVDC link(s). The supplementary bus is connected to the main bus through a very short AC link (i.e., very low inductance). These supplementary buses are shown in violet in Fig. 3. The following list includes other major preparatory steps:

- The active and reactive power limits (P_{max}, P_{min}, Q_{max} and Q_{min}) of conventional and wind generators are set to match the system documentation produced by Net-Op.

- The power factors of loads and wind plants are fixed to 0.8 and 0.9 respectively. It is of note that the wind plant power factor has an impact on the plant reactive power capability which affects its contribution in voltage support. In addition, reactive power limits of power electronics converters have a decisive influence.

- The control method used in HVDC corridors is Power-Voltage control [11]. One converter is responsible for matching a reference value of active power transmitted by the DC link (this mainly depends on the expected capacity factor of the connected WFC). The other end converter maintains the DC link rated voltage level. For the sake of consistency, the WFC-end converter is always power controlled.

- The reactive limits of converters are assumed to be +0.25 and -0.75 per unit from their rated capacities according to the real modern HVDC link fabricated by Siemens [12].
- The dynamics comprises detailed models for the HVDC Voltage Source Converters, wind turbine Type 4 generator and electrical models, and conventional generators are represented by round rotor model as shown in Table 3. The numerical values of the VSC model parameters are found in Table 4 in the Appendix.

Table 3. Types of dynamic models of the integrated generation assets.

Types of integrated models	
Wind turbines – Generator	'WT4G1'
Wind turbines – Converter	'WT4E1'
DC converter stations	'VSCDCT'
Synchronous generators	'GENROU'

3.2. Implying faults

Using PSS/E fault routine

The implemented case studies are designed to investigate the impact of the integrated WFCs on the voltage response of the connected grid areas during severe faults. In particular, each bus of the major four buses (i.e., 20, 30, 40 and 50; Cases A to D) suffers a solid three phase fault leading to a severe voltage dip. The voltage response at the faulted bus is compared to the voltage regime required by the grid code. In addition, the voltage responses at some selected buses, and power flows from the faulted bus are displayed prior, during and post the dip. Two different grid codes are integrated, namely, E.ON code and Norwegian code (Nord). Further details about the two codes are found in [13]. The fault is initiated at time = 1s, cleared after six cycles (i.e. system frequency is 50 Hz), and the simulations continue for 3 s.

Integration of user models

The concept of user model counts on forcing the faulted bust to follow the grid code regime at the instant of fault initiation. On the other hand, the responses of other buses and WFCs are monitored to be sure that they are still connected and fulfilling the code requirements. The PSS/E user-models are written in Fortran. The user-models were complied with whole model before starting the dynamic simulation as explained in the PSS/E documentation [14]. These models are designed to be as general as possible, in order to facilitate the adaptation of this procedure to future changes in the grid codes.

Bus 20 is selected to connect the user models which make the bus voltage follow E.ON and Nordic codes in two separate case studies. The concept of user models is also applied to examine the impact of a sudden phase shift and frequency step on the system performance, particularly, at Bus 20; 1) phase-shift step rise of 20 degrees, and 2) frequency step increase by 0.2 Hz, both occur at t = 0 s.

4. Results and discussions

4.1. Using PSS/E fault routine

The four cases proved to be coping with the grid codes, namely, Case A is compared to Nordic code as in Fig. 4-a, meanwhile Cases B to D are assessed against E.ON code as in Fig. 4-b. Most of the offshore WFCs (i.e., the operative and under commissioning or the far future) are connected through HVDC corridors. Thus, the reactive capability mainly depends on the reactive limits of the DC link inverter not on the wind turbines installed in the WFCs. It is also interesting to highlight the slight differences between the responses at the three buses in Fig. 4-b. Case D records a slow initial recovery, which might be due to the lower generation capacity connected at bus 50. Meanwhile, Bus 30 exploited a minor overshoot, where the high wind power penetration is a possible cause. Among the three responses, Case C achieved the best response since the voltage recovered very fast after the fault clearance with minimum oscillations and avoided any overshoots. Likewise, the response at Bus 20 is promising and there is an acceptable safe time-margin between the code requirements and the actual recovery after the voltage dip.

Next, separate analysis for each case study is conducted. The voltage responses at two near buses to the faulted bus are investigated, namely Buses 24 and 101 for Case A as shown in Fig. 5-a. Bus 24 is considerably affected as it has no generation, and close to the faulted bus, meanwhile Bus 101 is more robust as it is connected to WFC A. However, Bus 101 suffers minor oscillations before it stabilizes (this bus is also connected to an HVDC link). In Case B, Buses 361 and 24 are selected as shown in Fig. 5-b (Bus 361: the supplementary bus connecting the

offshore WFC at Bus 36). Bus 361 does not sense the voltage dip as it is connected to the grid only through HVDC links; but Bus 32 is slightly affected. The conventional generators' speeds are also displayed by Fig. 6-a. Cases A and C are characterized with very small deviations, but the corresponding figures are not included due to space limitations. However, Case B reached a speed dip of about 0.75 Hz, which might generate a frequency event in this area of the grid. But this dip continues for a very short duration with respect to the thresholds of dead-bands of frequency sensors. Thus, frequency support procedures should not be initiated.

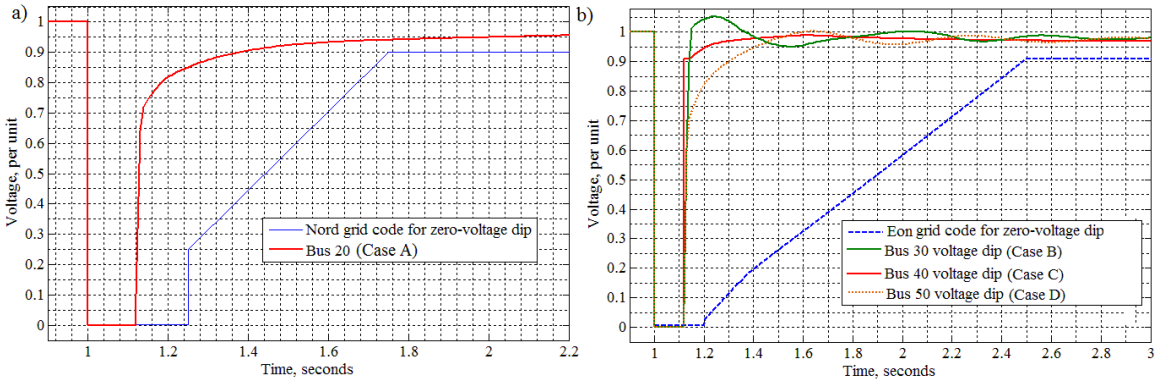

Fig. 4. (a) Case A voltage dip compared to Nord grid code; (b) Cases B to D voltage dips compared to E.ON grid code

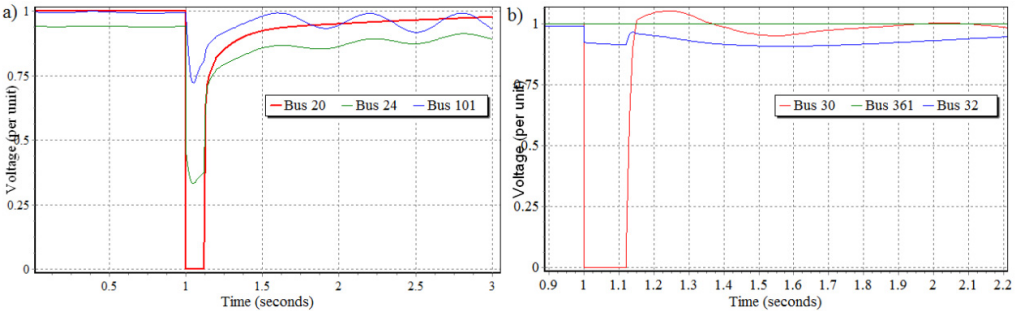

Fig. 5. (a) voltage responses of Cases A at different buses; (b) voltage responses of Cases B at different buses

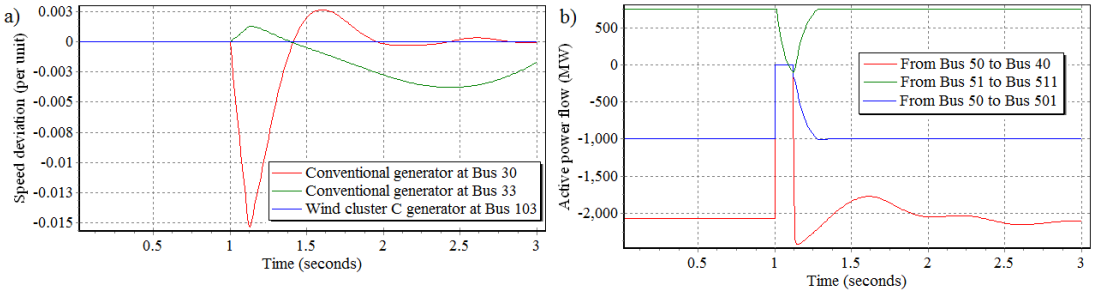

Fig. 6. (a) conventional generators speed deviations at Case B; (b) examples for power flow at Case D

In Fig. 6-b (Case D), the generation of WFC at Bus 51 is not delivered, hence the converter is forced to suppress the output gradually, and it builds up again after the fault is cleared. As an illustration, the output of Bus 51 is consumed mainly through Bus 50, but the fault avoided this consumption (i.e., the pre-set active power delivery of DC link between Buses 511 and 361 is maintained). It is of note that all the power flows through the bus are following the trend of wind generation building up at Bus 51, until the pre-fault values are retained. The recovery of normal operation for the flow through the AC link between Germany and Netherlands (Buses 40 and 50) is slower due to the huge conventional and renewable generation capacities integrated at both buses.

4.2. Integration of user models

In the case studies of Bus 20, simulations show that the fault affects only Buses 24 and 101; meanwhile the other buses are not affected as they are connected through HVDC corridors. This is illustrated through Fig. 7-a (Bus 102) and Fig. 8-b (Buses 101 and 103). The major difference between the two dips is in the first stage, where the Nordic code dip is severer (voltage drops to almost 0), therefore, other buses (i.e., 24 and 101) drop to the same level. Conversely, in E.ON case study, the voltage nadir is different between the three buses, where the worst deviation occurs at the faulted bus, namely, Bus 20. The reactive current grid requirement is fulfilled by the WFCs as shown in Fig. 8-a, where the reactive current is always higher than the red threshold. However, the reactive power slightly violates the code limit after the fault is almost cleared as shown in Fig. 8-b. It is of note that the tough spike in actual reactive power is most likely due to the iterative numerical issues of the PSS/E. Finally, a user model simulated a frequency rise by 0.2 Hz at Bus 20 that causes a continuous increase in absolute phase angles at the buses which are connected to Bus 20 (i.e. Bus 24 and 21). The sudden speed deviation between the voltage vector at Bus 20 and the corresponding voltage vectors at Buses 21 and 24 forced their phase angles to keep rising. The sudden rise of frequency forced the generator at Bus 20 to accelerate; so that its speed deviates from the nominal value by 0.004 per unit (0.2 Hz). The voltages and power delivered/consumed by these buses are almost unaffected (minor oscillations in the range of 0.0001 per unit) but their curves are not shown due to space limitations.

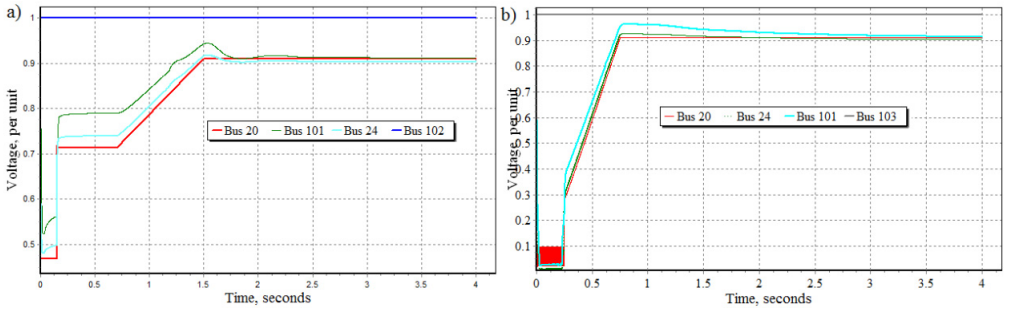

Fig. 7. voltage responses at several busses (a) E.ON voltage dip at Bus 20; (b) Nordic voltage dip at Bus 20

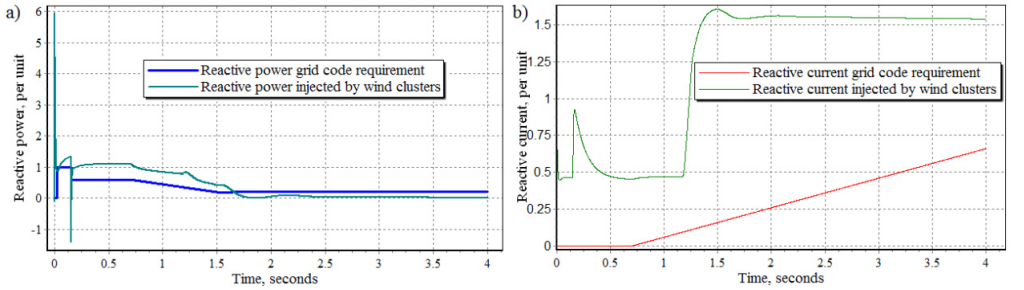

Fig. 8. voltage dip at bus 20: (a) actual reactive current vs. E.ON requirements; (b) actual reactive power vs. E.ON requirements

5. Conclusions

This paper investigates the impact of integrating three large offshore WFCs on the stability of certain grid. This grid connects the major synchronous areas which might be supplied by these clusters directly or indirectly through the AC lines or HVDC links. The Net-OP tool suggested an optimized topology to connect the WFCs to this grid to form a 15-bus benchmark system. The first step was to deal with the *.RAW file provided by Net-OP tool in the frame of DTOC project. Afterwards, a dynamic model for the whole system is prepared (*.DYR) to perform several case studies. Most of the case studies represented severe voltage dips at main buses. The grid code compliance at the faulted bus and the nearby buses is investigated. All the case studies proved an acceptable pattern for voltage recovery after the faults. However, the converters of HVDC failed in some cases to provide the required reactive

current to the nearby faulted bus because the converters' models in PSS/E are not equipped with the suitable control algorithms. The integrated grid codes are designed for WFCs which are connected through the AC lines; hence the voltage support capabilities are mainly based on WFCs/WTGs reactive power limits. In the case of offshore WFCs which are connected through HVDC links, voltage support is related to the control methods and ratings of the power electronic converters of the HVDC link. Thus, comprehensive efforts are required to design new grid codes which specify clearly the role of HVDC links in providing ancillary services, including voltage and frequency support during unusual events. In future, Special attention should be paid to the dynamic modelling of the converters in HVDC links, because the play a critical role in the provision of reactive current during voltage dips. In addition, advanced user models could be implemented to provide the converters the capability of voltage support.

Appendix

Table 4 Numerical values for VSC-HVDC model in PSS/E

VSCDCT			
J Tpo_1, Time constant of active power order controller, sec (VSC # 1).	0.05	J+14 AC_VC_Limits_2, Reactive power limit for ac voltage control, pu on converter MVA rating	0
J+1 AC_VC_Limits_1, Reactive power limit for ac voltage control, pu on converter MVA rating	0	J+15 AC_Vctrl_kp_2, AC Voltage control proportional gain, converter MVA rating/BASEKV (VSC#2).	2.4
J+2 AC_Vctrl_kp_1, AC Voltage control proportional gain, converter MVA rating/BASEKV (VSC # 1).	2.4	J+16 Tac_2 > 0.0, Time constant for AC voltage PI integral, sec (VSC#2). When 0, VSC#2 is ignored.	0.01
J+3 Tac_1 > 0, Time constant for AC voltage PI integral, sec (VSC#1).	0.01	J+17 Tacm_2, Time constant of the ac voltage transducer, sec (VSC#2), *must be longer than simulation step*	0.05
J+4 Tacm_1, Time constant of the ac voltage transducer, sec (VSC # 1), *must be longer than simulation step*	0.05	J+18 Iacmax_2, Current Limit, pu on converter MVA rating (VSC#2).	1
J+5 Iacmax_1, Current Limit, pu on converter MVA rating (VSC#1).	1	J+19 Droop_2, AC Voltage control droop, converter MVA rating/BASEKV (VSC#2).	0
J+6 Droop_1, AC Voltage control droop, converter MVA rating/BASEKV (VSC#1).	0	J+20 VCMX_2, Max. VSC Bridge Internal Voltage (VSC#2).	1.07
J+7 VCMX_1, Max. VSC Bridge Internal Voltage (VSC#1).	1.07	J+21 XREACT_2 > 0.0, Pu reactance of the ac series reactor on converter MVA rating (VSC# 2)	0.17
J+8 XREACT_1 > 0.0, Pu reactance of the ac series reactor on converter MVA rating (VSC#1).	0.17	J+22 QMAX_2, Max. system reactive limit in MVAR (VSC#2).	240
J+9 QMAX_1, Max. system reactive limits in MVAR (VSC#1)	240	J+23 QMIN_2, Min. system reactive limits in MVAR (VSC#2).	-740
J+10 QMIN_1, Min. system reactive limits in MVAR (VSC#1).	-740	J+24 AC_VC_KT_2, feedback from reactive power limiter to ac voltage controller (VSC#2)	1.2
J+11 AC_VC_KT_1, feedback from reactive power limiter to ac voltage controller (VSC#1).	1.2	J+25 AC_VC_KTP_2, feedback from current order limiter to ac voltage controller (VSC#2).	1
J+12 AC_VC_KTP_1, feedback from current order limiter to ac voltage controller (VSC#1).	1	J+26 Tpo_DCL, Time constant of the power order controller, sec (DC Line).	0.05
J+13 Tpo_2, Time constant of active power order controller, sec (VSC#2).	0.05	J+27 Tpo_lim, Time constant of the power order limit controller, sec (DC Line).	0.05

The full codes of the implemented user models (*.FLX script files) are available in [13].

References

[1] I.E.A. (IEA), World Energy Outlook, in, International Energy Agency, Paris, 2012.
[2] Z. Xu, M. Gordon, M. Lind, J. Ostergaard, Towards a Danish Power System with 50% Wind — Smart Grids Activities in Denmark, in: IEEE Power & Energy Society General Meeting, Lyngby, 2009.
[3] H. Holttinen, A.G. Orths, *et al.*, Currents of changes, IEEE Power and Energy Magazine, 9 (2011) 47-59.
[4] M. Tsili, S. Papathanassiou, A review of grid code technical requirements for wind farms, Renewable Power Generation, 3 (2009) 308-332.
[5] W. Ye, H. Bayem, *et al.*, Methods for assessing available wind primary power reserve, IEEE Trans. on Sustainable Energy, 6 (2015) 272-280.
[6] I. Machado, I. Arias, Grid Codes Comparison, in: ElectricPower Engineering, Chalmers University of Technology, 2006.
[7] European Energy Reasearch Alliance, EERA-DTOC, in, European Energy Research Alliance, Copenhagen, 2012 (http://www.eera-dtoc.eu/)

[8] H.G. Svendsen, Planning Tool for Clustering and Optimised Grid Connection of Offshore Wind Farms, Deepwind'2013 - Selected Papers from 10th Deep Sea Offshore Wind R&D Conference, 35 (2013) 297-306.
[9] J.T.G. Pierik, U. Axelsson, E. Eriksson, D. Salomonsson, EeFarm II Description, testing and application, in, Delft, Netherlands, 2009.
[10] M.A. Parker, O. Anaya-Lara, Cost and losses associated with offshore wind farm collection networks which centralise the turbine power electronic converters, Iet Renewable Power Generation, 7 (2013) 390-400.
[11] Lecture: VSC-HVDC, Course: FACTS and HVDC in Electric Power Systems, in, Royal Institute of Technology (KTH), Sweden, 2012.
[12] M. Davies, M. Dommaschk, *et al.*, HVDC PLUS – Basics and Principle of Operation, in: E.S. Siemens AG (Ed.), Germany, 2011.
[13] O. Anaya-Lara and P. Ledesma, "D2.5 Procedure for Verification of Grid Code Compliance," European Energy Research Alliance, Copenhagen, 2012 (http://www.eera-dtoc.eu/wp-content/uploads/files/D2_5-Procedure-for-Verificationof-Grid-Code-Compliance.pdf)
[14] Siemens, Power, Technologies, International, PSS®E Documentation, in, Siemens Industry, Inc., 2012.